Cobalt(I) Pincer Complexes as Catalysts for CO_2 Hydrogenation to Formate

Wenzhi Yao,[a] Gbolagade Olajide,[b] Chance M. Boudreaux,[a] Megan M. Wysocki,[a] Md. Kausar Ahmed,[a] Fengrui Qu,[a, c] Tibor Szilvási,[b]* and Elizabeth T. Papish[a]*

[a] Department of Chemistry and Biochemistry, University of Alabama, Shelby Hall, Tuscaloosa, Alabama 35487, United States

[b] Department of Chemical and Biological Engineering, University of Alabama, Tuscaloosa, Alabama 35487, United States

[c] Current Address: Department of Chemistry, University of Michigan, Ann Arbor, Michigan 48109, United States

* Corresponding Authors

Email addresses:

tibor.szilvasi@ua.edu

etpapish@ua.edu

ABSTRACT

Carbon dioxide hydrogenation with base to generate formate salts can provide a means of storing hydrogen in an energy dense solid. However, this application requires catalytic CO_2 hydrogenation, which would ideally use an earth abundant metal catalyst. In this article, six new (CNC)$Co^{I}L_2$ pincer complexes were synthesized and fully characterized, including single crystal X-Ray diffraction analysis on four new complexes. These complexes contain an imidazole-based (**1_R**) N-heterocyclic carbene (NHC) ring or a benzimidazole based NHC ring (**2_R**) in the CNC pincer. The R group is para to N on the pyridine ring and been varied from electron withdrawing (CF_3) to donating (Me, OMe) substituents. The L type ligands have included CO and phosphine ligands (in **$^{PPh3}2$** and **$^{PMe3}2$**). Thus, two known Co complexes (**1**, **1_{OMe}**) and six new complexes (**1_{Me}**, **1_{CF3}**, **2**, **2_{OMe}**, **$^{PPh3}2$**, **$^{PMe3}2$**) were studied for the CO_2 hydrogenation reaction. In general, the unsubstituted CNC pincer complexes bearing two carbonyl ligands led to the highest activity. The best catalyst, **2**, remains active for over 16 h and produces a turnover number of 39,800 with 20 bars of 1:1 CO_2 / H_2 mixture at 60 °C. A computational study of the mechanism of CO_2 hydrogenation is also reported.

TOC Graphic

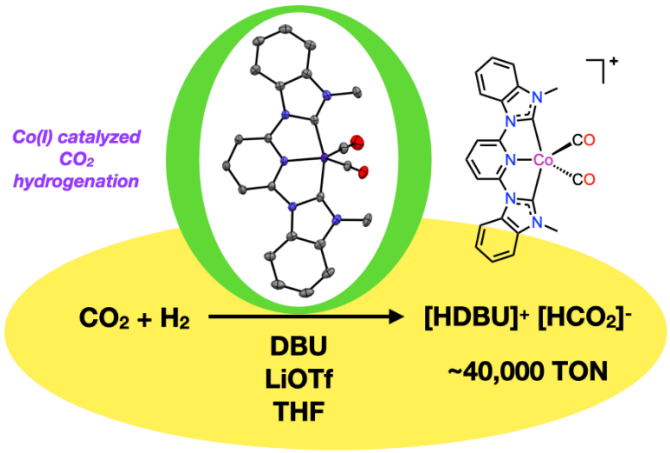

Keywords: Cobalt(I), hydrogenation, pincer ligands, carbon dioxide reduction, N-heterocyclic carbenes.

INTRODUCTION

The combustion of fossil fuels contributes to global warming due to increasing levels of CO_2 in the atmosphere.[1] Carbon dioxide also represents an abundant carbon source which could be used for hydrogen storage.[2-3] Carbon dioxide hydrogenation in the presence of base (e.g. $NaHCO_3$) typically leads to formate salts (e.g. sodium formate) which can be used to store hydrogen in an energy dense solid.[4-7] (Scheme 1) These formate salts can be used as hydrogen storage materials with hydrogen and CO_2 release upon acidification of the compounds.[8]

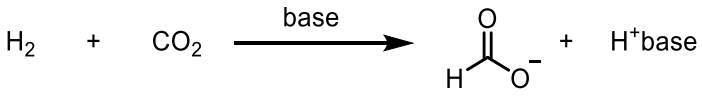

Scheme 1. CO_2 hydrogenation and to produce formate salts

The development of the homogeneous CO_2 hydrogenation has made significant progress in the past 30 years and has been summarized in several reviews.[6, 9-13] Several reports have used homogeneous catalysts based upon precious metals including Ir, Ru, Pd, and Rh.[14-26] For example, Nozaki's PNP iridium(III) catalyst (**Lit-1**, Figure 1) achieves 3.5×10^6 turnovers (TON) for CO_2 hydrogenation to form potassium formate.[14] However, iridium is one of the rarest elements in the Earth's crust. A more sustainable process can be envisioned by using earth abundant 3d transition elements for catalytic CO_2 hydrogenation and Mn,[27] Fe,[28] Co,[29-31] Ni[32] and Cu[33-34] complexes have been used as homogeneous catalysts for this reaction. Hazari and Bernskoetter reported that the (PNP)Fe(II) catalyst (**Lit-2**, Figure 1) hydrogenates CO_2 in the presence of the base 1,8-diazabicycloundec-7-ene (DBU) with nearly 60,000 TON due to rate acceleration from a Lewis acid (LiOTf) and metal-ligand cooperativity involving the nitrogen of the PNP ligand.[28] Similarly, the (PNP)Co(I) complex **Lit-3** (Figure 1) also takes advantage of the same factors (DBU and LiOTF) to produce 29,000 TON for CO_2 hydrogenation.[29]

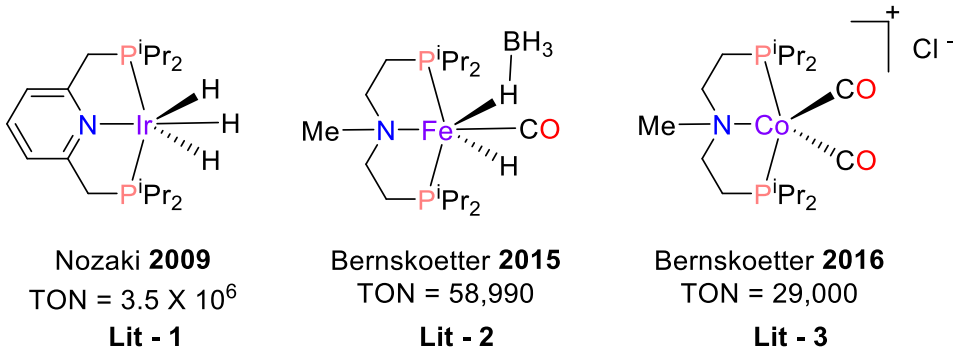

Figure 1. Previous examples of CO_2 hydrogenation.

We recently reported cobalt(I) and nickel (II) CNC pincer complexes that are active catalysts for photochemical CO_2 reduction via sacrificial electrons and protons to form CO and/or formate.[35-37] The CNC pincer ligand was derived from pyridine and N-heterocyclic carbene (NHC) donor groups wherein the pyridine electronic properties can be modulated by changing the substituent *para* to nitrogen.[38-39] We speculated that these cobalt(I) complexes may be viable catalysts for thermal CO_2 hydrogenation.

In this report, a series of Co(I) CNC pincer complexes (Figure 2) were synthesized and studied for CO_2 hydrogenation. The "**1**" series of compounds uses an imidazole derived NHC ring whereas the "**2**" series has a benzimidazole derived NHC ring in the CNC pincer. In our $^{L}\mathbf{1}_{R}$ and $^{L}\mathbf{2}_{R}$ nomenclature, L (when present) is the ligand that replaces a CO on cobalt(I) and R is the *para* substituent on the pyridine ring of the CNC pincer. Two of the complexes (**1** and $\mathbf{1}_{OMe}$) were previously reported.[35] Six of the complexes are new including $\mathbf{1}_{Me}$, $\mathbf{1}_{CF3}$, **2**, $\mathbf{2}_{OMe}$, $^{PPh3}\mathbf{2}$, and $^{PMe3}\mathbf{2}$. All eight complexes were studied herein for the CO_2 hydrogenation reaction to produce formate.

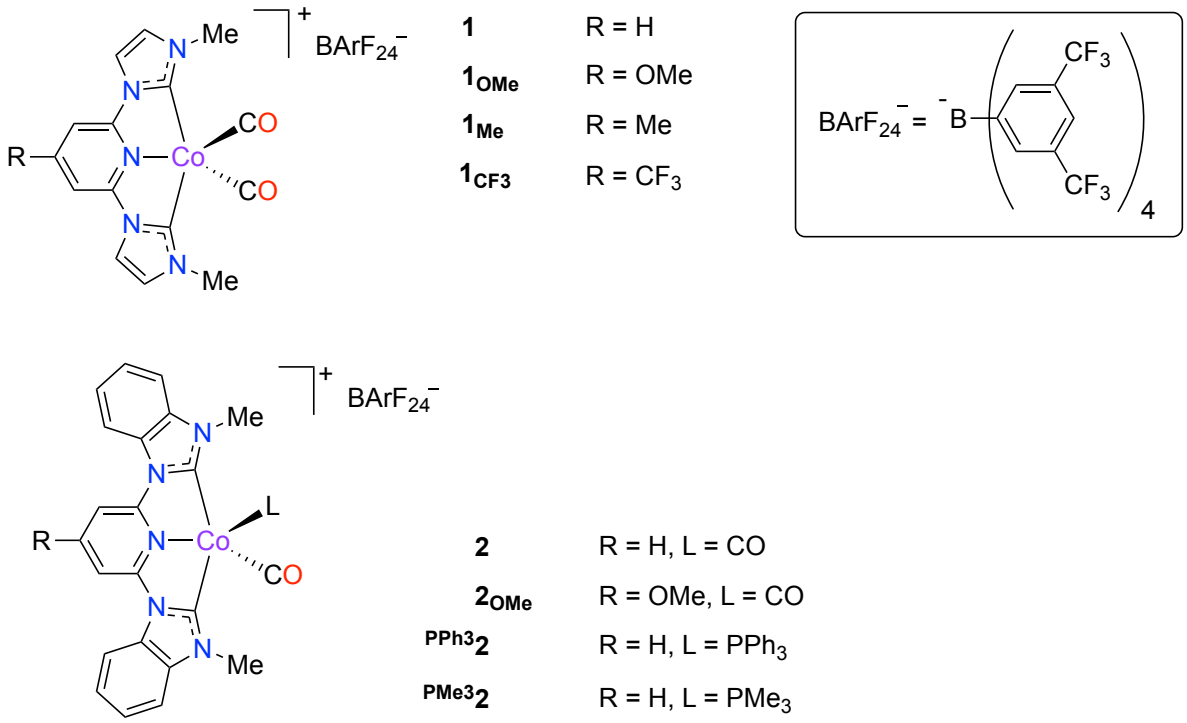

Figure 2. Structures of Co(I) CNC pincer catalysts used for CO_2 hydrogenation.

Results and Discussion

Synthesis. The synthesis of the cobalt(I) complexes (Figure 2) followed the procedures previously developed in the group.[35] Each preligand (**L1$_R$(HOTf)$_2$** and **L2$_R$(HOTf)$_2$**) was deprotonated with triethylamine in presence of $Co_2(CO)_8$ to make corresponding **1$_R$′** and **2$_R$′** complexes (Scheme 2). This disproportionation of $Co_2(CO)_8$ yielded the Co(I) CNC pincer complexes and a $[Co(CO)_4]^-$ anion (as the major product with some $[OTf]^-$ present) as observed in our prior publication and in the literature with other ligands.[35, 40-41] To avoid the presence of two Co sources during catalysis, a salt metathesis with sodium tetrakis(3,5-trifluoromethyl)phenyl)-borate ($NaBArF_{24}$) was performed to obtain pure **1$_R$** and **2$_R$** with the $BArF_{24}$ anion. Catalysts of type **1$_R$** and **2$_R$** were synthesized with a wide variety of R groups (R = H, OMe, Me, and CF_3 for **1$_R$** and R = H and

OMe for $\mathbf{2_R}$) to test both electron donating and withdrawing substituents. The yields of complexes $\mathbf{1_R}$ and $\mathbf{2_R}$ are reported in Scheme 2 and the supporting information and they range from 8 to 52% for two steps. With complex **2** (R = H), we also substituted one CO ligand with triphenyl phosphine ($^{PPh3}\mathbf{2}$, >99% yield) or trimethyl phosphine ($^{PMe3}\mathbf{2}$, >99% yield). These compounds were characterized by ^{1}H, ^{13}C, ^{19}F, and ^{31}P (for phosphine complexes) NMR, IR, and high res. MS or elemental analysis as described in the experimental section and the supporting information. Crystallographic data is reported for selected complexes as described below.

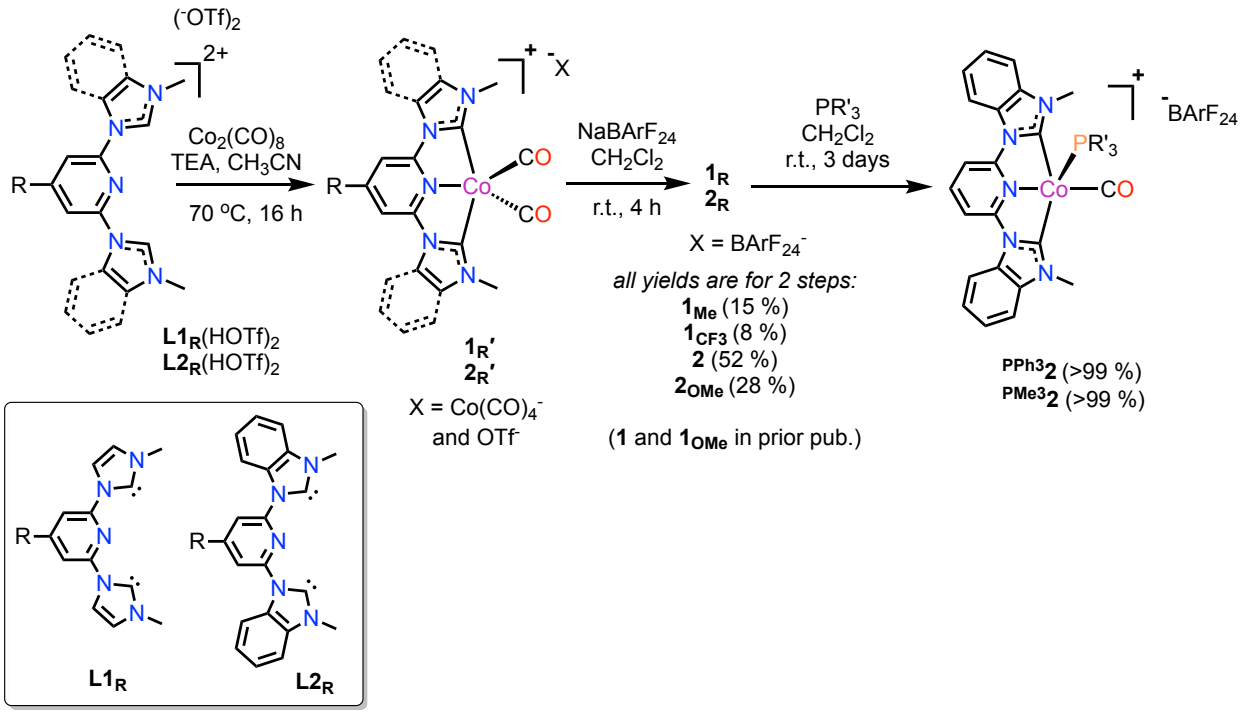

Scheme 2. Synthesis of cobalt(I) complexes used for CO_2 hydrogenation.

Single Crystal X-ray Diffraction. Crystals suitable for single crystal X-ray diffraction were obtained for $\mathbf{2_{OMe}}$ by slow evaporation of diethyl ether with a drop of acetonitrile. The other crystals were obtained by layering hexanes on top of either a concentrated solution of **2** or $^{PPh3}\mathbf{2}$ in

diethyl ether or a concentrated solution of ^{PMe3}**2** in dichloromethane. The structures of the complexes are shown in Figure 3 with a view of the primary coordination sphere to emphasize the change in geometry at the metal center upon phosphine coordination. The geometry index value τ_5 was also calculated and shown below each structure.[42] The parameter τ_5 ranges from 0 to 1, with the extreme values corresponding to a perfect square pyramid and a perfect trigonal bipyramid, respectively. As shown in Figure 3 and Table 1, all the dicarbonyl complexes have τ_5 values in the range around ~0.5 to 0.6 (including previously published values for **1** and $\mathbf{1}_{OMe}$). These distortions from trigonal bipyramid geometry are due to the chelate ring constraints, and do not represent distortions towards a square pyramid geometry since the carbonyl ligands are both equidistant from the plane of the pincer ligand. Compared to the dicarbonyl complex **2** (τ_5 = 0.559), its phosphine derivatives ^{PPh3}**2** (τ_5 = 0.284) and ^{PMe3}**2** (τ_5 = 0.222) are closer to a square pyramid geometry. This geometry change creates a free site *trans* to phosphine on the metal center.

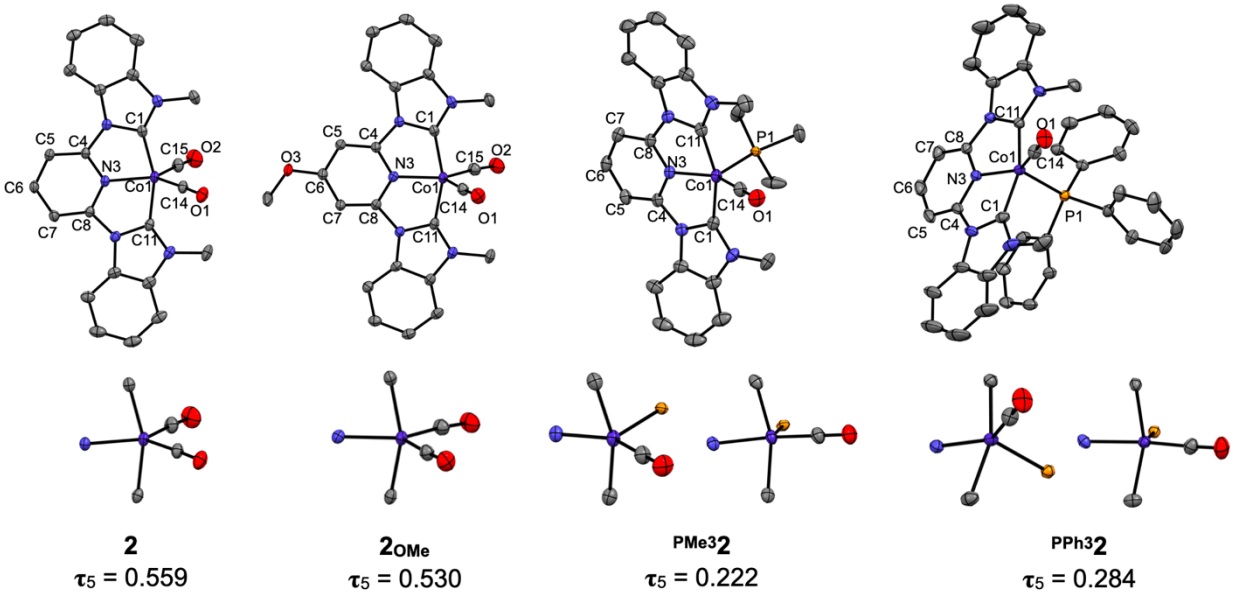

Figure 3. Molecular diagram of the new cobalt(I) complexes based on crystallographic data with hydrogen atoms and the $BArF_{24}$ anions removed for clarity. The cobalt first coordination sphere is

also shown for each complex along with the τ_5 parameter. Thermal ellipsoids are drawn at the 50% probability level.

As shown in Table 1, the Co-C(NHC) bond length decreased slightly from the imidazole derived complexes (**1_R**) to the benzimidazole complexes (**$^{L}2_R$**). The other distances around the metal center (Co-CO and Co-N) were similar across the series of dicarbonyl complexes. The substitution of one CO ligand for a phosphine results (in **$^{PMe3}2$** and **$^{PPh3}2$**) in a shortened Co-CO distance by ~0.04 Å which may be due to enhanced back bonding due to a more electron rich metal. The C6-O3 distance in **2^{OMe}** is 1.343(2) Å which shows that the methoxy group has partial double bond character due to resonance; similar bond distances have been noted in other methoxy substituted pincer complexes.[35, 38, 43-44]

Table 1. Selected bond lengths, angles, and τ_5 parameter for Co(I) complexes.[a] Complexes **1** and $\mathbf{1_{OMe}}$ were reported in a prior publication and are shown here for comparison.[35]

Designation	**1**	$\mathbf{1_{OMe}}$	**2**	$\mathbf{2_{OMe}}$	^{PPh3}**2**	^{PMe3}**2**
bond angles (°)						
N3−Co1−$C_{NHC\text{-}avg}$	79.4(1)	79.3(1)	79.72(6)	79.67(7)	80.05(6)	80.25(6)
N3−Co1−$C_{CO\text{-}avg}$	125.4(1)	125.2(1)	123.90(7)	124.33(8)	142.55(6)	146.14(6)
N3−Co1−P1					102.53(4)	104.09(8)
C14−Co1−L[b]	109.2(2)	109.7(1)	112.08(7)	111.3(1)	114.90(5)	109.76(9)
C1−Co1−C11	158.8(1)	158.6(1)	159.28(6)	159.28(8)	159.59(6)	159.43(6)
τ_5	0.548	0.545	0.559	0.530	0.284	0.222
bond lengths (Å)						
Co1−$C_{NHC\text{-}avg}$	1.922(4)	1.914(3)	1.888(1)	1.894(2)	1.884(2)	1.876(1)
Co1−N3	1.916(3)	1.918(2)	1.908(1)	1.919(1)	1.902(1)	1.897(1)
Co1−$C_{CO\text{-}avg}$	1.775(4)	1.775(4)	1.786(2)	1.769(2)	1.743(1)	1.743(2)
Co1−P1					2.2483(4)	2.236(3)
C_{CO}−$O_{CO\text{-}avg}$	1.145(6)	1.144(6)	1.138(2)	1.143(3)	1.153(1)	1.151(2)

[a]Averages are used when applicable. [b]L = C15 or P1 depending on respective metal bounded atom.

Vibrational Spectroscopy. Complexes **1** and $\mathbf{1_{OMe}}$ were previously studied by FTIR spectroscopy.[35] The dicarbonyl Co(I) cations have C_{2v} symmetry (Table 2 entries 1-6) and show A_1 symmetric carbonyl stretches of weak intensity between 2011 and 2034 cm^{-1} and B_2 asymmetric carbonyl stretches of strong intensity between 1958 and 1982 cm^{-1}. The phosphine substituted Co(I) cations (Table 2 entries 7 and 8) have C_s symmetry and only one carbonyl stretch is observed and is assigned as an A' vibrational mode. These phosphine complexes display a much lower CO stretch (at 1948-1949 cm^{-1}) than the dicarbonyl complexes (at 1958-2034 cm^{-1}) which reflects the electron donation from phosphine to the Co(I) center which allows for substantial backbonding to CO. For both type **1** (imidazole derived) and type **2** (benzimidazole derived) complexes, changing the R group on the pyridine ring from H to OMe (in **1** vs. $\mathbf{1_{OMe}}$ or **2** vs. $\mathbf{2_{OMe}}$) increased the electron density at metal center for more back bonding to CO and decreased the carbonyl stretch by 10 – 21 cm^{-1}. It appears that Me and OMe are similarly electron donating, as $\mathbf{1_{Me}}$ and $\mathbf{1_{OMe}}$ display similar CO stretches. In contrast, changing the R group from H to the more electron withdrawing CF_3 has no influence on the A_1 stretch but it increased the B_2 mode by 9 cm^{-1} which is consistent with a less electron rich metal.

Table 2. Carbonyl stretching frequencies collected via FTIR-ATR for Co(I) complexes.

Entry	Complex	Carbonyl Frequencies [cm^{-1}]
1	**1**[a]	2025 (A_1), 1968 (B_2)
2	$\mathbf{1_{OMe}}$ [a]	2011 (A_1), 1958 (B_2)
3	$\mathbf{1_{Me}}$	2012 (A_1), 1960 (B_2)
4	$\mathbf{1_{CF3}}$	2025 (A_1), 1977 (B_2)
5	**2**	2034 (A_1), 1982 (B_2)
6	$\mathbf{2_{OMe}}$	2013 (A_1), 1962 (B_2)
7	$^{PPh3}\mathbf{2}$	1949 (A')
8	$^{PMe3}\mathbf{2}$	1948 (A')

[a] The values were previously reported.[35]

CO_2 hydrogenation. CO_2 hydrogenation reactions were studied by using a Parr reactor pressurized with 1:1 CO_2 and H_2. The reactions were run in tetrahydrofuran (THF) solution containing Co complex, lithium triflate (LiOTf) as a Lewis acid, and 1,8-diazabicyclo[5.4.0]undec-7-ene (DBU) as base to trap the product generated by the CO_2 hydrogenation (Scheme 3). While the role of DBU has been discussed and debated in the literature,[45] the current consensus is that DBU acts as a base and does not bind CO_2. In dry solvent, there is no evidence for a zwitterionic complex forming between DBU and CO_2.[46]

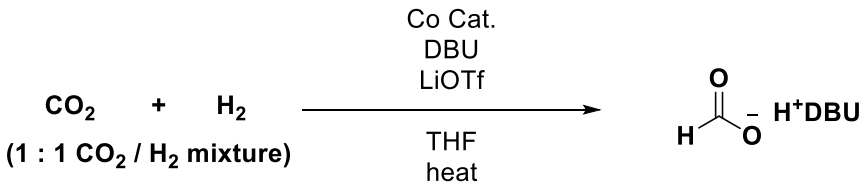

Scheme 3. CO_2 hydrogenation reaction catalyzed by Co(I) CNC pincer complex.

Several control experiments were run initially to determine the extent of background reaction in the absence of a catalyst (Table 3). The product ($HDBU^+$ HCO_2^-) is isolated in small amounts in the absence of cobalt or in the presence of a cobalt anion source (entries 1 and 2, respectively). Entry 2 shows that $NaCo(CO)_4$ produces less product than no cobalt catalyst, and thus shows no rate acceleration.

Table 3. Control experiments for CO_2 hydrogenation to form $[HDBU]^+[HCO_2]^-$.[a]

Entry	Catalyst	LiOTf	$[HDBU]^+[HCO_2]^-$
1	N/A	0.32 mmol	40(3) μmol
2	0.3 μmol of $NaCo(CO)_4$	0.32 mmol	32(5) μmol

[a]All experiments were done in triplicate. Conditions: Parr reactor was pressurized with 40 bars of CO_2 / H_2 mixture and 4.8 mmol of DBU and heated at 80 °C for 4 h after placing reaction mixture into the reactor in glovebox. Reaction mixture was prepared in 5 mL THF. See the Supporting Information for further details.

With control experiments completed, we tested eight catalysts for CO_2 hydrogenation in the presence of LiOTf and DBU (Table 4). These results show that with the imidazole derived NHC rings, catalyst **1** is most active with 11,000 TON. Surprisingly, any R group substitution within $\mathbf{1_R}$ catalysts gives a slight decrease in activity to ~3,000 to 4,000 TON for $\mathbf{1_{OMe}}$, $\mathbf{1_{Me}}$, and $\mathbf{1_{CF3}}$. We suggest that this trend is due to side reactions that lead to catalyst decomposition for $\mathbf{1_R}$ derivatives, with possible decomposition pathways involving reactivity at the R group or hydrogenation of the aromatic ring within the CNC pincer.[47] A similar trend was observed between **2** and $\mathbf{2_{OMe}}$ (14,900 vs. 2,200 TON, respectively). Overall comparing **1** vs. **2** and $\mathbf{1_{OMe}}$ vs. $\mathbf{2_{OMe}}$, there is no clear trend with respect to benzimidazole vs. imidazole derived NHC rings, but **2** is the best catalyst of the group. Phosphine substitution for CO appears to decrease the TON values from 14,900 (**2**) to 12,000 ($\mathbf{^{PMe3}2}$) or 6,900 ($\mathbf{^{PPh3}2}$) (entries 8 and 9), but phosphine is not as detrimental as R group substitution on the pyridine ring. With the reasons for these trends being unclear, we proceeded with further experiments on **2** given that **2** is the best catalyst. Using these same conditions but stopping the reaction at different time points for analysis, it is apparent that the

catalyst **2** is most active at the beginning of the reaction but it maintains activity for the full 16 hours (Table 5 and Figure 4).

Table 4. Catalyst activity for CO_2 hydrogenation.[a]

Entry	Complex	TON ($\times 10^3$)[b]
1	**1**	11(2)
2	$\mathbf{1}_{\mathbf{OMe}}$	3.8(9)
3	$\mathbf{1}_{\mathbf{Me}}$	2.74(7)
4	$\mathbf{1}_{\mathbf{CF3}}$	4.2(6)
5	**2**	14.9(9)
6	$\mathbf{2}_{\mathbf{OMe}}$	2.2(8)
7	$^{\mathbf{PMe3}}\mathbf{2}$	12(2)
8	$^{\mathbf{PPh3}}\mathbf{2}$	6.9(9)

[a]All experiments were done in triplicate or quadruplicate and were analyzed by ^{1}H NMR. Conditions: Parr reactor was pressurized with 40 bars of CO_2 / H_2 mixture and heated at 80 °C for 4 h after placing reaction mixture into the reactor in glovebox. Reaction mixture contains 6 μM Co complex, 0.384 M DBU, 64 mM LiOTf in THF solution. See the Supporting Information for further details. [b]Turnover number is calculated based on DMF internal standard added while preparing the NMR sample.

Table 5. Influence of reaction time.[a]

Entry	Time (h)	TON (×10^3)[b]
1	1	2.5(3)
2	2	5.3(1)
3	4	8.5(9)
4	8	11.0(3)
5	16	14(1)

[a]All experiments were done in triplicate or quadruplicate and were analyzed by ^{1}H NMR. Conditions: Parr reactor was pressurized with 40 bars of CO_2 / H_2 mixture and heated at 80 °C after placing reaction mixture into the reactor in glovebox. Reaction mixture contains 45.5 μM Co complex **2**, 1.92 M DBU, 64 mM LiOTf, and in THF solution. See the Supporting Information for further details. [b]Turnover number is calculated based on DMF internal standard added while preparing NMR sample.

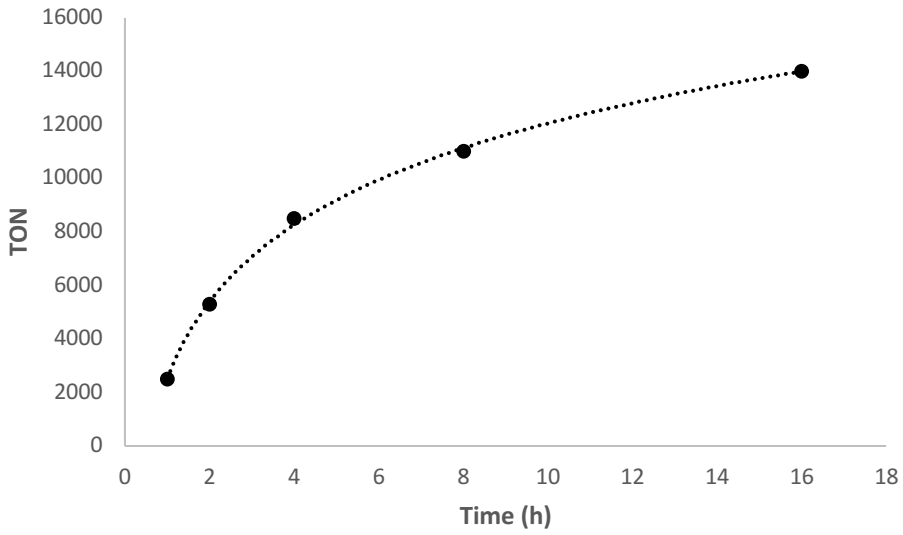

Figure 4. Turnover numbers with different reaction times for complex **2**.

Further studies on catalyst **2** were performed by varying the pressure and the temperature of the reaction (Table 6). Keeping the temperature constant at 80 °C and varying the pressure in entries 1-6 showed that 20 bar was the optimal pressure of 50/50 CO_2 and H_2. This may represent a compromise between having sufficient reactants, but too high a pressure may inhibit CO loss which would be necessary to generate a free site for catalysis. In entries 7-10, we used constant pressure and varied the temperature, which showed that 60 °C was optimal. This may represent a compromise between having sufficient activation energy, but avoiding high temperatures which may lead to decomposition. A full study of the initial rates as a function of temperature and measuring catalyst spectra before and after the reaction would be necessary to clarify this temperature dependence, however this is beyond the scope of the current work.

Table 6. The influence of pressure and temperature with catalyst **2**.[a] The optimal TON values were obtained with the conditions highlighted in red.

Entry	**Pressure (bar)**	**Temperature (°C)**	**TON ($\times 10^3$)[b]**
1	60	80	5.9(4)
2	40	80	8.5(9)
3	30	80	10.0(3)
4	20	80	22(1)
5	10	80	7.2(5)
6	5	80	6.5(5)
7	40	100	9.7(7)
8	40	60	21(3)
9	40	40	4.0(4)

10	40	22	4.1(4)

[a]All experiments were done in triplicate or quadruplicate and were analyzed by ^{1}H NMR. Conditions: Parr reactor was pressurized with CO_2 / H_2 mixture and heated for 4 h accordingly after placing reaction mixture into the reactor in glovebox. Reaction mixture contains 45.5 μM Co complex **2**, 1.92 M DBU, 64 mM LiOTf, in THF solution. See the Supporting Information for further details. [b]Turnover number is calculated based on DMF internal standard added while preparing NMR sample.

With these optimized conditions, the reaction was run on larger scale with 32.5 μM of complex **2**, 91.4 mM of LiOTf, and 2.7 M of DBU in 3.5 mL of THF solution under 20 bars of 1:1 CO_2 / H_2 mixture and heated at 60 °C for 16 h. The best TON observed for complex **2** under these conditions was $3.98(8) \times 10^4$.

Mechanism and Computational Results. Using the above information along with studies of similar catalysts in the literature,[27-29, 48] we can propose a mechanism for CO_2 hydrogenation. The initial $[(CNC)Co(CO)_2]^+$ complex (e.g. **1** or **2)** is an 18 e- complex, which must lose a CO ligand to enable H_2 binding. The 16e- $[(CNC)Co(CO)]^+$ complex can bind H_2 to form a Co(I)-η^2-H_2 complex or a Co(III) dihydride, both of which have 18 electrons. Deprotonation with DBU then leads to a cobalt(I) hydride, [(CNC)Co(CO)H], which is poised to nucleophilically attack CO_2. The resulting formate complex can be O bound or H bound. Formate dissociation then returns to the $[(CNC)Co(CO)]^+$ intermediate. The optimal rate involving intermediate pressure of CO_2/H_2 suggests that CO dissociation is required. Rate acceleration in the presence of Lewis acids has generally been attributed to Li^+ binding to formate and assisting in formate dissociation.[27-28, 48]

We calculated the catalytic cycle of CO_2 hydrogenation using **1** as a catalyst (Figure 5) and find a plausible reaction mechanism. To initiate the catalytic cycle, **1** loses a CO ligand to form

INT1. This reaction is endergonic (reaction free energy, ΔG_r = 8.0 kcal/mol) and has no electronic energy barrier according to our potential energy surface scan. The catalytic cycle starts with H_2 coordination that is a barrierless and slightly endergonic step (INT2, ΔG_r = 2.2 kcal/mol). Next, DBU deprotonates INT2, forming a cobalt hydride complex (INT3) in an exergonic step (ΔG_r = -5.9 kcal/mol). This reaction step has a 10.4 kcal/mol free energy barrier relative to INT2 and 20.6 kcal/mol barrier relative to **1**, which indicates that this reaction step can occur under the experimentally applied catalytic conditions (60 °C).

CO_2 can then react with the cobalt hydride, INT3, to form a weakly-bound H-coordinated Co-formate complex (INT4). INT4 has a zwitterionic resonance structure that can be stabilized by a neighboring ion. Thus, we consider three ways how this reaction step can proceed: (i) no ion coordination (INT4), (ii) with $[HDBU]^+$ coordination (INT4'), and (iii) with Li^+ coordination (INT4"). Without any ion coordination, the formation of INT4 is highly endergonic (ΔG_r = 10.5 kcal/mol) while subsequent formate release is slightly exergonic (ΔG_r = -3.2 kcal/mol). Formate release formally closes the catalytic cycle; however, this reaction is uphill relative to INT1 by 3.6 kcal/mol hence it is not thermodynamically feasible. In the presence of $[HDBU]^+$, the energetics are more favorable. The formation of INT4' is also highly endergonic (ΔG_r = 11.9 kcal/mol) but release of the formate $[HDBU]^+$ complex is highly exergonic (ΔG_r = -10.5 kcal/mol). The catalytic cycle is now slightly exergonic (-2.3 kcal/mol), hence it is favorable thermodynamically. As a third option, we also analyze the effect of Li^+. This pathway is very strongly exergonic. The formation of INT4" is highly exergonic (ΔG_r = -19.9 kcal/mol) and Li-formate formation is another barrierless and highly exergonic step (ΔG_r = -14.6 kcal/mol). We note that INT4" can isomerize to an alternate structure, in which formate is coordinated through O rather than H. This structure is 6.1 kcal/mol downhill from INT4" but uphill relative to Li-formate formation by 8.5 kcal/mol, thus

we do not show it in Figure 5. The overall catalytic cycle is highly favorable when Li^+ is present (-38.2 kcal/mol) and the strong thermodynamic driving force also explains the lack of an energy barrier in these steps. We expect that there is a free energy barrier due to entropic effects in the formation of INT4" that involves the association of multiple species; however, we presume this barrier is small when Li^+ is present given the high thermodynamic driving force. We note that as the reactions go to completion (e.g. $3.98(8) \times 10^4$ TON corresponds to 1.3 M of formate produced), the quantity of LiOTf (91.4 mM) will be limited and formate stabilization by $[HDBU]^+$ (from 2.7 M of DBU used) will play a greater role.

Our results demonstrate that the proposed mechanism for CO_2 hydrogenation on catalyst **1** is kinetically feasible and thermodynamically favorable in the presence of DBU and LiOTf explaining the high observed TON values. Our results also suggest that the role of LiOTf is in stabilizing the cobalt-formate intermediate and promoting formate release from the catalyst, making the step kinetically viable and thermodynamically favorable.

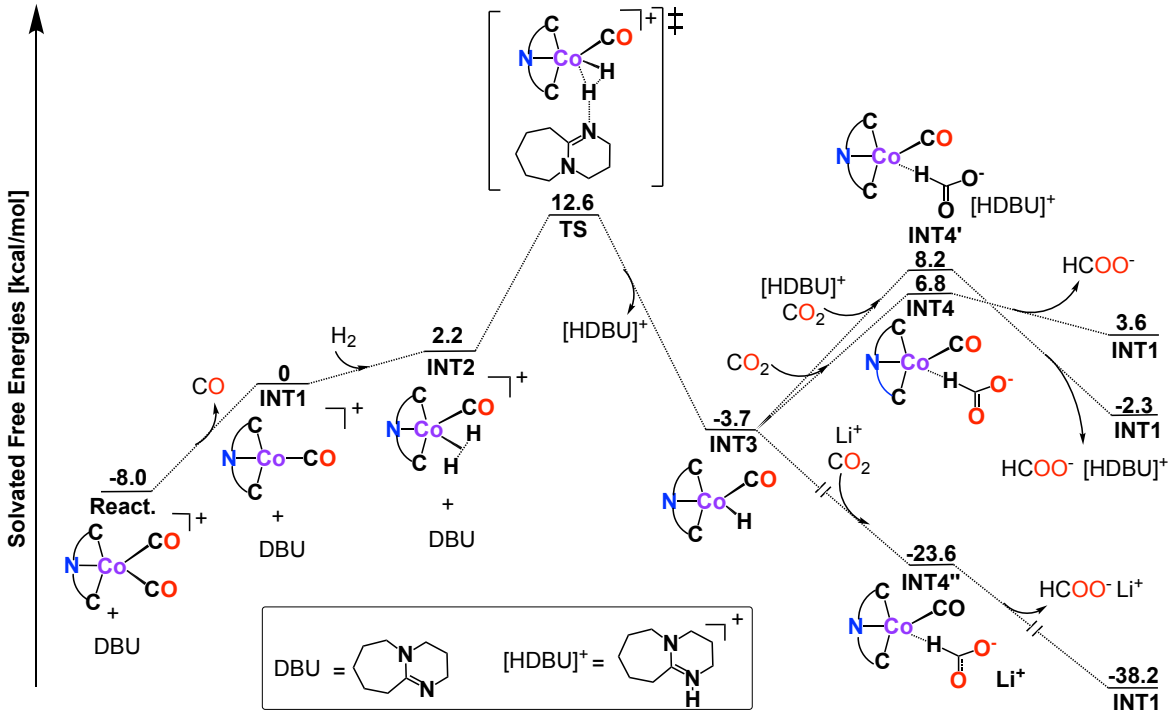

Figure 5. A DFT derived reaction mechanism for CO_2 hydrogenation using **1** as catalyst. All calculations were done at the DLPNO-CCSD(T)(SMD=THF)/def2-TZVPP//ωB97X-D(SMD=THF)/def2-SVP level of theory. See the supporting information (.xyz) for cartesian coordinates of all optimized stationary points.

Experimental

General considerations. Reactions were prepared and performed under an inert atmosphere (N_2) using glovebox or Schlenk line techniques in oven dried glassware unless otherwise stated. Work up and purifications were done open to air except cobalt containing compounds. All the cobalt containing compounds were worked up and purified under an inert atmosphere (N_2).

Solvents and reagents. Dry solvents (either commercial or dried on a glass contour solvent purification system built by Pure Process Technology, LLC) were used for reactions unless described otherwise. Reagent grade solvents were used for work up and purification. All the reagents were used as received from the commercial supplier without further purification.

Instruments and Services. NMR spectra were recorded using a Bruker AVANCE 360 (360 MHz, ^{1}H frequency) or an AVANCE 500 (500MHz, ^{1}H frequency) NMR spectrometer. FT-IR spectra were recorded in a Bruker Alpha ATR-IR spectrophotometer. Mass spectra were obtained in a Waters AutoSpec-Ultima NT mass spectrometer or Waters Xero G2-XS QTOF. Elemental analyses were done by Atlantic Microlab, Inc. and Robertson Microlit Laboratories.

NMR chemical shift reference. ^{1}H and $\{^1H\}^{13}$C chemical shifts were assigned with respect to the residual peaks from deuterated NMR solvents.[49] No reference was used for ^{19}F and ^{31}P chemical shifts, only the number of peaks were checked.

Synthesis of $\mathbf{1_{Me}}$ precursor ($\mathbf{1_{Me}'}$). In a Schlenk flask, 1,1'-(4-methylpyridine-2,6-diyl)bis(3-methyl-1*H*-imidazol-3-ium) trifluoromethanesulfonate ($\mathbf{L1_{Me}}(HOTf)_2$, 588 mg, 2.30 mmol) and

$Co_2(CO)_8$ (398 mg, 1.16 mmol) were added under inert atmosphere (Scheme 2). A solution of triethylamine in acetonitrile (0.8 mL, 0.36 M) was added with stirring. An additional 14 mL MeCN was added. Bubbles were formed while stirring. The reaction mixture was heated to 70 °C for 16 h. The reaction was cooled to room temperature and concentrated *in vacuo* after heating. The residue was then washed with Et_2O. The product was recovered by filtration and dried under vacuum overnight. Complex $\mathbf{1_{Me}}$ precursor was obtained as yellow solid (217 mg, the counter ion is a mixture of $[Co(CO)_4]^-$ and $[OTf]^-$). ^{1}H-NMR (DMSO-d_6, 500 MHz, ppm): δ 8.63 (d, 2H, J = 1.9 Hz), 8.10 (s, 2H), 7.78 (d, 2H, J = 1.9 Hz), 3.93 (s, 6H), 2.67 (s, 3H).

Synthesis of $\mathbf{1_{Me}}$. In a vial, $\mathbf{1_{Me}'}$ (144 mg, ~0.247 mmol) and dichloromethane (DCM, 2.5 mL) were added (Scheme 2). A solution of sodium tetrakis[3,5-bis(trifluoromethyl)phenyl]borate (241 mg 0.272 mmol) in DCM (2.5 mL) was added in 3 portions to the vial with stirring. The reaction was stirred overnight at room temperature. White precipitate formed during the reaction. The result reaction mixture was filtered over Celite, and the Celite plug was rinsed with 1 mL additional DCM. The combined solution was then concentrated *in vacuo*. The residue was washed with hexanes and dried under vacuum overnight. Product was obtained as yellow powder, and the yield is 265 mg (0.215 mmol, 15.2 % for 2 steps). ^{1}H-NMR (DMSO-d6, 500 MHz, ppm): δ 8.62 (d, 2H, J = 2.3 Hz), 8.10 (d, 2H, J = 0.4 Hz), 7.78 (d, 2H, J = 2.2 Hz), 7.72 (s, 4H), 7.61 (t, 8H, J = 2.2 Hz), 3.93 (s, 6H), 2.66 (s, 3H). ^{19}F-NMR (DMSO-d6, 471 MHz, ppm): δ -61.61. $\{^1H\}^{13}$C-NMR (DMSO-d6, 126 MHz, ppm) δ 195.8 (s, C_{NCN}), 184.1 (s, C_{CO}), 160.9 (q, $J_{C,B}$ = 50.3 Hz, $C_{ipso\text{-}BArF}$), 151.1 (s, $C_{p\text{-}py}$), 147.7 (s, $C_{o\text{-}py}$), 134.0 (s, $C_{o\text{-}BArF}$), 128.5 (q, $J_{C,F}$ = 31.9 Hz, $C_{m\text{-}BArF}$), 126.3 (s, C_{im}), 124.0 (q, $J_{C,F}$ = 276.8 Hz, $C_{CF3\text{-}BArF}$), 117.7 (s, C_{im}), 117.5 (s, $C_{p\text{-}BArF}$), 107.0 (s, $C_{m\text{-}py}$), 45.7 (s, $C_{Me\text{-}p\text{-}py}$), 37.2 (s, C_{NMe}). HRMS (ESI) calculated for $CoC_{15}H_{15}N_5O$ (M-$BArF_{24}$-CO): 340.0609, found 340.0619. HRMS (ESI) calculated for $C_{32}H_{12}BF_{24}$ ($BArF_{24}$): 863.0649, found 863.0643.

FT-IR (ATR, cm^{-1}): 2012, 1960, 1933, 1643, 1610, 1558, 1541, 1491, 1414, 1352, 1274, 1160, 1117, 1029, 947, 927, 885, 833, 794, 746, 714, 697, 679, 667, 639, 578, 560, 531, 498, 456, 420, 409.

Synthesis of 1,1'-(4-trifluoromethylpyridine-2,6-diyl)bis(3-methyl-1*H*-imidazol-3-ium)chloride. In a pressurized tube, added 2,6-Dichloro-4-(trifluoromethyl)pyridine (250 mg, 1.157 mmol) and 1-methylimidazole (603 mg, 11.6 mmol) with a stir bar (Scheme 4). The reaction was sealed and heated at 150 °C for 1 h. The crude product was partially precipitated out. The reaction mixture was dissolved in methanol (2 mL), and diethyl ether (10 mL) was added to get the product precipitated out of the solution as off white solid. The solid was collected by a vacuum filtration, and washed with diethyl ether (20 mL). Yield of the product is 187.8 mg (42.7 %). ^{1}H-NMR (DMSO-d6, 500 MHz, ppm): δ 10.86 (s, 2H), 8.92 (t, 2H, J = 1.9 Hz), 8.72 (s, 2H), 8.07 (t, 2H, J = 1.8 Hz), 4.05 (s, 6H).

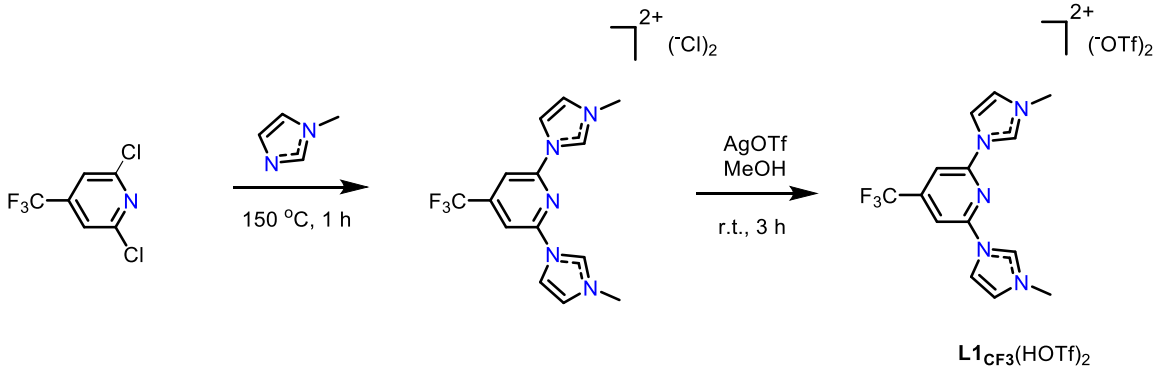

Scheme 4. Synthesis of $\mathbf{L1_{CF3}}(HOTf)_2$.

Synthesis of 1,1'-(4-trifluoromethylpyridine-2,6-diyl)bis(3-methyl-1*H*-imidazol-3-ium)triflate, ($\mathbf{L1_{CF3}(HOTf)_2}$). In round bottom flask, added 1,1'-(4-trifluoromethylpyridine-2,6-diyl)bis(3-methyl-1*H*-imidazol-3-ium)chloride (150 mg, 0.395 mmol) and methanol (2 mL) with a stir bar (Scheme 4). While stirring, silver triflate (203.0 mg, 0.790 mmol) was added in form of

powder. The reaction was continue stirred for 3 h. The precipitates were filtered off, and the filtrate was concentrated to generate the crude product. The crude product was then washed with dichloromethane to yield the pure product as a white solid (197.6 mg, 82.4 %) ^{1}H-NMR (DMSO-d6, 500 MHz, ppm): δ 10.66 (s, 2H), 8.88 (t, 2H, *J* = 2.2 Hz), 8.70 (s, 2H), 8.08 (t, 2H, *J* = 1.9 Hz), 4.04 (s, 6H). ^{19}F-NMR (DMSO-d6, 471 MHz, ppm): δ -63.02, -77.75.

Synthesis of $\mathbf{1}_{CF3}$ precursor ($\mathbf{1}_{CF3}$'). In a Schlenk flask, 1,1'-(4-trifluoromethylpyridine-2,6-diyl)bis(3-methyl-1*H*-imidazol-3-ium)triflate (**L1**$_{CF3}$(HOTf)$_2$, 170 mg, 0.280 mmol) and $Co_2(CO)_8$ (138 mg, 0.363 mmol) were added under inert atmosphere (Scheme 2). A solution of triethylamine in acetonitrile (4.5 mL, 0.36 M) was added with stirring. Bubbles were formed while stirring. The reaction mixture was heated to 70 °C for 16 h. The reaction was cooled to room temperature and concentrated *in vacuo* after heating. The residue was then washed with Et_2O. The product was recovered by filtration and dried under vacuum overnight. Complex $\mathbf{1}_{CF3}$ precursor was obtained as yellow solid (143 mg, the counter ion is a mixture of $[Co(CO)_4]^-$ and $[OTf]^-$). ^{1}H-NMR (DMSO-d6, 500 MHz, ppm): δ 8.83 (s, 2H), 8.74 (s, 2H), 7.84 (s, 2H), 3.98 (s, 6H). ^{19}F-NMR (DMSO-d6, 471 MHz, ppm): δ -61.64, -77.75.

Synthesis of $\mathbf{1}_{CF3}$. In a vial, $\mathbf{1}_{CF3}$' (143 mg, ~0.250 mmol) and dichloromethane (DCM, 1.5 mL) were added. A solution of sodium tetrakis[3,5-bis(trifluoromethyl)phenyl]borate (222 mg 0.250 mmol) in DCM (1.5 mL) was added in 3 portions to the vial with stirring (Scheme 2). The reaction was stirred overnight at room temperature. White precipitate formed during the reaction. The result reaction mixture was filtered over Celite, and the Celite plug was rinsed with 1 mL additional DCM. The combined solution was then concentrated *in vacuo*. The residue was washed with hexanes and dried under vacuum overnight. The product was obtained as reddish yellow powder. (30 mg, 0.023 mmol, 8.0 % for 2 steps) ^{1}H-NMR (DMSO-d6, 500 MHz, ppm): δ 8.84 (s, 2H), 8.74

(s, 2H), 7.84 (s, 2H), 7.73 (s, 4H), 7.62 (s, 8H), 3.98 (s, 6H). ^{19}F-NMR (DMSO-d6, 471 MHz, ppm): δ -61.61. {^{1}H}^{13}C-NMR (DMSO-d6, 126 MHz, ppm) δ 195.0 (s, C_{NCN}), 184.2 (s, C_{CO}), 160.9 (q, $J_{C,B}$ = 50.4 Hz, $C_{ipso\text{-}BArF}$), 148.2 (s, $C_{o\text{-}py}$), 136.3 (q, $J_{C,F}$ = 34.0 Hz, $C_{p\text{-}py}$), 134.0 (s, $C_{o\text{-}BArF}$), 128.5 (q, $J_{C,F}$ = 31.5 Hz, $C_{m\text{-}BArF}$), 126.6 (s, C_{im}), 124.0 (q, $J_{C,F}$ = 273.4 Hz, $C_{CF3\text{-}BArF}$), 118.0 (s, C_{im}), 117.7 (s, $C_{p\text{-}BArF}$), 103.1 (s, $C_{m\text{-}py}$), 45.7 (s, $C_{CF3\text{-}p\text{-}py}$), 37.3 (s, C_{NMe}). HRMS (ESI) calculated for $CoC_{16}H_{12}N_5O_2F_3$ (M-$BArF_{24}$): 422.0275, found 422.0281. HRMS (ESI) calculated for $C_{32}H_{12}BF_{24}$ ($BArF_{24}$): 863.0649, found 863.0646. FT-IR (ATR, cm^{-1}): 3101, 2025, 1977, 1948, 1897, 1878, 1610, 1559, 1542, 1493, 1466, 1416, 1398, 1353, 1272, 1115, 1039, 947, 929, 889, 855, 838, 794, 746, 713, 681, 668, 639, 580, 547, 529, 490, 465, 448, 424.

Synthesis of 2 precursor (2'). In a Schlenk flask, 1,1'-(pyridine-2,6-diyl)bis(3-methyl-1*H*-imidazol-3-ium) trifluoromethanesulfonate (**L2**$(HOTf)_2$, 500 mg, 0.782 mmol) and $Co_2(CO)_8$ (381 mg, 1.00 mmol) were added under inert atmosphere (Scheme 2). A solution of triethylamine in acetonitrile (10 mL, 0.36 M) was added with stirring. Bubbles were formed while stirring. The reaction mixture was heated to 70 °C for 16 h. The reaction was cooled to room temperature and concentrated *in vacuo* after heating. The residue was then washed with Et_2O. The product was recovered by filtration and dried under vacuum overnight. Complex **2** precursor was obtained as yellow solid (275 mg, the counter ion is a mixture of $[Co(CO)_4]^-$ and $[OTf]^-$). ^{1}H-NMR (DMSO-d6, 500 MHz, ppm): δ 8.61 (b, 5H), 7.98 (b, 2H), 7.66 (b, 4H), 4.23 (s, 6H). ^{19}F-NMR (DMSO-d6, 471 MHz, ppm): δ -77.77.

Synthesis of 2. In a vial, **2'** (200 mg, ~0.330 mmol) and dichloromethane (DCM, 5 mL) were added. A solution of sodium tetrakis[3,5-bis(trifluoromethyl)phenyl]borate (293 mg 0.330 mmol) in DCM (5 mL) was added in 3 portions to the vial with stirring (Scheme 2). The reaction was stirred overnight at room temperature. White precipitate formed during the reaction. The result

reaction mixture was filtered over Celite, and the Celite plug was rinsed with 1 mL additional DCM. The combined solution was then concentrated *in vacuo*. The residue was washed with hexanes and dried under vacuum overnight. The product was obtained as yellow powder (401 mg, 0.304 mmol, 51.7 % for 2 steps). ^{1}H-NMR (DMSO-d6, 500 MHz, ppm): δ 8.64 – 8.58 (m, 4H), 8.58 – 8.51 (m, 1H), 8.01 – 7.95 (m, 2H), 7.73 (s, 4H), 7.70 – 7.65 (m, 4H), 7.63 (t, 8H, J = 2.7 Hz), 4.23 (s, 6H). ^{19}F-NMR (DMSO-d6, 471 MHz, ppm): δ -61.59. {^{1}H}^{13}C-NMR (DMSO-d6, 126 MHz, ppm) δ 197.4 (s, C_{NCN}), 195.3 (s, C_{CO}), 160.9 (q, $J_{C,B}$ = 50.4 Hz, $C_{ipso\text{-}BArF}$), 148.4 (s, $C_{p\text{-}py}$), 139.4 (s, $C_{o\text{-}py}$), 135.9 (s, C_{Bzim}), 134.0 (s, $C_{o\text{-}BArF}$), 130.3 (s, C_{Bzim}), 128.5 (q, $J_{C,F}$ = 31.5 Hz, $C_{m\text{-}BArF}$), 125.1 (s, C_{Bzim}), 124.7 (s, C_{Bzim}), 124.0 (q, $J_{C,F}$ = 273.4 Hz, $C_{CF3\text{-}BArF}$), 117.8 (s, $C_{p\text{-}BArF}$), 112.4 (s, C_{Bzim}), 111.8 (s, C_{Bzim}), 107.2 (s, $C_{m\text{-}py}$), 34.8 (s, C_{NMe}). Anal. Calcd. For $C_{55}H_{29}BCoF_{24}N_5O_2$: C, 50.14; H, 2.22; N, 5.32. Found: C, 50.02; H, 1.93; N, 5.12. FT-IR (ATR, cm^{-1}): 2034, 1982, 1602, 1574, 1491, 1465, 1449, 1408, 1353, 1274, 1215, 1186, 1112, 1091, 1019, 931, 898, 887, 839, 808, 769, 741, 711, 681, 670, 647, 625, 595, 550, 523, 488, 462, 449, 425.

Synthesis of $\mathbf{2_{OMe}}$ precursor ($\mathbf{2_{OMe}'}$). In a Schlenk flask, 1,1'-(4-(methoxy)pyridine-2,6-diyl)bis(3-methyl-1*H*-imidazol-3-ium) trifluoromethanesulfonate ($\mathbf{L2_{OMe}}(HOTf)_2$, 0.493 g, 0.736 mmol) and $Co_2(CO)_8$ (0.948 mg, 2.495 mmol) were added under inert atmosphere (Scheme 2). A solution of triethylamine in acetonitrile (25 mL, 0.36 M) was added with stirring. Bubbles were formed while stirring. The reaction mixture was heated to 70 °C for 16 h. The reaction was cooled to room temperature and concentrated *in vacuo* after heating. The residue was then washed with dichloromethane (DCM) until the solid was bright yellow and the filtrate was pale in color. Complex $\mathbf{2_{OMe}}$ precursor was obtained as yellow solid (0.186 g, 0.284 mmol, 39%). ^{1}H-NMR (DMSO-d6, 360 MHz, ppm): δ 8.67 (d, 2H, J = 7.9 Hz), 8.00 (s, 2H), 7.96 (d, 2H, J = 7.0 Hz), 7.65 (q, 4H, J = 7.2 Hz), 4.34 (s, 3H), 4.22 (s, 6H). {^{1}H}^{13}C-NMR (DMSO-d6, 126 MHz, ppm) δ

198.7 (s, C_{NCN}), δ 196.2 (s, C_{CO}), δ 169.5 (s, $C_{p\text{-}py}$), δ 149.6 (s, $C_{o\text{-}py}$), δ 136.4 (s, C_{Bzim}), δ 130.6 (s, C_{Bzim}), δ 125.6 (s, C_{Bzim}), δ 125.1 (s, C_{Bzim}), δ 113.1 (s, C_{Bzim}), δ 112.1 (s, C_{Bzim}), δ 94.8 (s, $C_{m\text{-}py}$), δ 58.4 (s, C_{OMe}), δ 35.3 (s, C_{NMe}) FT-IR (ATR, cm^{-1}): CO(%T): 2023 (m), 1964 (s); $[Co(CO)_4]^-$: 1862 (br-vs).

Synthesis of $\mathbf{2_{OMe}}$. A round bottom flask was charged with complex $\mathbf{2_{OMe}'}$ (0.107 g, 0.163 mmol) and filled with dichloromethane (15 mL) resulting in a yellow solution. With stirring, sodium tetrakis-[1,3-bis(trifluoromethyl)phenyl]borate (147.34 g, 0.166 mmol) was added to the solution (Scheme 2). The resulting solution was stirred for 4 h. resulting in the formation of a white precipitate. The mixture was filtered over celite and the plug was rinsed further with dichloromethane (DCM) until the filtrate was colorless. The filtrate was evaporated to dryness in vacuo leaving a yellow residue, $\mathbf{2_{OMe}}$ (0.159, 0.118 mmol, 72%). ^{1}H-NMR (DMSO-d6, 360 MHz, ppm): δ 8.64 (d, 2H, J = 7.7 Hz), 7.96 (s, 2H), 7.93 (d, 2H, J = 8.2 Hz), 7.70 (s, 4H), 7.62 (q, 4H, J = 9.1 Hz), 7.62 (s, 8H), 4.33 (s, 3H), 4.20 (s, 6H) ^{19}F-NMR (DMSO-d6, 339 MHz, ppm): δ -61.65. {^{1}H}^{13}C-NMR (DMSO-d6, 126 MHz, ppm) δ 198.8 (s, C_{NCN}), δ 196.1 (s, C_{CO}), δ 169.5 (s, $C_{p\text{-}py}$), δ 161.4 (q, J = 50.6 Hz, $C_{ipso\text{-}BArF}$), δ 149.6 (s, $C_{o\text{-}py}$), δ 136.4 (s, C_{Bzim}), δ 134.5 (s, $C_{o\text{-}BArF}$), δ 130.6 (s, C_{Bzim}), δ 128.9 (q, J = 33.7 Hz, $C_{m\text{-}BArF}$), δ 125.6 (s, C_{Bzim}), δ 125.0 (s, C_{Bzim}), δ 124.2 (q, J = 273.2 Hz, $C_{CF3\text{-}BArF}$), δ 118.1 (s, $C_{p\text{-}BArF}$), δ 113.1 (s, C_{Bzim}), δ 112.0 (s, C_{Bzim}), δ 94.8 (s, $C_{m\text{-}py}$), δ 58.3 (s, C_{OMe}), δ 37.2 (s, C_{NMe}) Anal. Calcd. for $C_{56}H_{31}BCoO_3F_{24}N_5$: C, 49.91; H, 2.32; N, 5.20. Found: C, 48.37; H, 2.28; N, 5.04, we note that the discrepancy in the elemental analysis results may be due to air sensitivity. FT-IR (ATR, cm^{-1}): CO(%T): 2013 (m), 1962 (s).

Synthesis of $^{PPh3}\mathbf{2}$. In a vial, **2** (198 mg, 0.15 mmol) and dichloromethane (DCM, 2 mL). The solution was stirred and the triphenyl phosphine (157 mg, 0.600 mmol) was added (Scheme 2). After stirring over 3 days, the solution had become a clear red. The solvent was removed to half

volume and hexane was added dropwise with vigorous stirring. A red precipitate formed, and hexane was added continually until the solvent was colorless or nearly colorless. The precipitate was collected on a frit and washed several times with hexanes to yield the product as a red powder. (236 mg, 0.152 mmol, quantitative) ^{1}H-NMR (DMSO-d6, 500 MHz, ppm): δ 8.49 – 8.41 (m, 4H), 8.39 – 8.34 (m, 1H), 7.73 (s, 4H), 7.66 – 7.58 (m, 10H), 7.58 – 7.50 (m, 4H), 7.23 (td, 3H, *J* = 7.5 Hz, *J* = 1.4 Hz), 7.05 (td, 6H, *J* = 7.6 Hz, *J* = 1.6 Hz), 6.68 (td, 6H, *J* = 9.1 Hz, *J* = 1.8 Hz), 3.59 (d, 6H, *J* = 1.1 Hz). ^{19}F-NMR (DMSO-d6, 338.83 MHz, ppm): δ -61.55. ^{31}P-NMR (DMSO-d6, 202 MHz, ppm): δ 31.63. {^{1}H}^{13}C-NMR (DMSO-d6, 126 MHz, ppm) δ 202.2 (d, *J* = 10.1), 160.9 (q, *J* = 50.3 Hz), 146.9 (d, *J* = 3.8 Hz), 136.2 (d, *J* = 2.5 Hz), 136.1 (d, *J* = 3.8 Hz), 134.0 (s), 133.2 (d, *J* = 32.7 Hz), 131.1 (d, *J* = 12.6 Hz), 129.8 (s), 129.7 (s), 128.5 (qq, *J* = 31.5 Hz, *J* = 2.5 Hz), 128.5 (d, *J* = 8.8 Hz), 124.8 (s), 124.0 (q, *J* = 271.7 Hz), 124.0 (s), 117.8 (s), 111.3 (d, *J* = 114.5 Hz), 106.0 (s), 54.9 (s), 33.8 (s). Anal. Calcd. For $C_{72}H_{44}BCoF_{24}N_5OP$: C, 55.73; H, 2.86; N, 4.51. Found: C, 55.64; H, 2.60; N, 4.47. FT-IR (ATR, cm^{-1}): 3852, 3749, 3075, 1949, 1609, 1569, 1492, 1479, 1439, 1400, 1352, 1325, 1272, 1181, 1111, 1092, 1030, 1017, 999, 956, 933, 884, 838, 815, 804, 762, 745, 735, 712, 697, 680, 670, 647, 618, 595, 551, 522, 503, 490, 466, 449, 428.

Synthesis of ^{PMe3}2. In a vial, **2** (198 mg, 0.15 mmol) and dichloromethane (DCM, 2 mL). The solution was stirred and the trimethyl phosphine (45.65 mg, 0.600 mmol) was added (Scheme 2). After stirring over 3 days, the solution had become a clear red. The solvent was removed to half volume and hexane was added dropwise with vigorous stirring. A red precipitate formed, and hexane was added continually until the solvent was colorless or nearly colorless. The precipitate was collected on a frit and washed several times with hexanes to yield the product as a red powder. (208 mg, 0.152 mmol, quantitative) ^{1}H-NMR (DMSO-d6, 500 MHz, ppm): δ 8.54 (d, 2H, *J* = 7.4 Hz), 8.50 (d, 2H, *J* = 7.9 Hz), 8.38 – 8.30 (m, 1H), 7.85 (d, 2H, *J* = 7.7 Hz), 7.73 (s, 4H), 7.65 –

7.52 (m, 12H), 4.20 (s, 6H), 0.78 (d, 9H, J = 8.6 Hz). ^{19}F-NMR (DMSO-d6, 338.83 MHz, ppm): δ -61.55. ^{31}P-NMR (DMSO-d6, 202 MHz, ppm): δ -4.11. {^{1}H}^{13}C-NMR (DMSO-d6, 126 MHz, ppm) δ 204.3 (d, J = 13.8), 160.9 (q, J = 50.3 Hz), 146.2 (s), 136.3 (s), 134.3 (s), 134.0 (s), 129.9 (s), 128.5 (q, J = 31.5 Hz), 124.1 (d, J = 138.4 Hz), 124.0 (q, J = 273.0 Hz), 117.8 (s), 111.8 (s), 111.0 (s), 105.5 (s), 54.9 (s), 34.7 (s), 16.8 (d, J = 22.6 Hz). Anal. Calcd. For $C_{57}H_{38}BCoF_{24}N_5OP$: C, 50.13; H, 2.80; N, 5.13. Found: C, 48.88; H, 2.54; N, 4.80, we note that the discrepancy in the elemental analysis results may be due to air sensitivity. FT-IR (ATR, cm^{-1}): 2961, 1948, 1791, 1612, 1595, 1558, 1491, 1478, 1441, 1399, 1354, 1327, 1275, 1113, 1028, 941, 898, 887, 838, 813, 763, 741, 712, 681, 668, 647, 618, 597, 579, 551, 533, 501, 466, 447, 425, 411.

General Co_2 Hydrogenation Procedures. In each test tube, 365.4 mg DBU, 0.5 mL LiOTf solution (1.2481 g, 8 mmol in 50 mL THF), 0.75 mL catalyst solution (5 μmol Co catalyst in 50 mL THF) were added. The reactions were stirred for 15 min or more before placing the test tubes into Parr reactor. The tubing was purged by 50 : 50 H_2 / CO_2 mixture before pressurizing the Parr reactor. The Parr reactor was purged 7 times with 50 : 50 H_2 / CO_2 mixture between 40 bar and 10 bar. The Parr reactor was then pressurized to the desired pressure. Heating time was recorded after the temperature reached target reaction temperature. After reaction, the reactor was removed from heating source, and cooled in ice / water bath to below 15 °C before depressurizing the reactor. For each reaction, 100 μL DMF was added as internal standard, followed by 0.5 – 1 mL D_2O to form a homogeneous solution or suspension. The mixture was stirred for at least 5 min. A sample was taken and diluted with D_2O for NMR analysis.

Computational Methods. We perform all density functional theory (DFT) calculations with Gaussian 16[50] and use ORCA 5.0.4[51] for domain-based local pair natural orbital coupled-cluster theory[52] (DLPNO-CCSD(T)) calculations. We performed a conformer search for each stationary

point using the GFN2-xTB[53] semi-empirical method in CREST[54] as implemented in the xTB program[55] (Version 6.7.0) and the most stable conformer is supplied for further DFT calculations. To account for solvation effects, we use the SMD model.[56] The reaction mechanism and related energetics are calculated at the DLPNO-CCSD(T)(SMD=THF)/def2-TZVPP//ωB97X-D(SMD=THF)/def2-SVP[57-58] level of theory. We tested low and high spin states for each stationary point and found that the low spin state is more favorable in every case. We confirm all stationary points by a normal mode analysis. Calculations also consider experimental reaction conditions. Using GoodVibes,[59] we correct all computed energetics from gas phase standard state to experimental reaction concentrations and conditions: temperature of 333 K, 20 bars of 1:1 CO_2/H_2, 32.5 μM of catalyst, 91.4 mM of LiOTf, and 2.7 M of DBU. Optimized cartesian coordinates (.xyz) are provided in the Supporting Information (SI).

Single Crystal X-Ray Diffraction (SC-XRD) Structure Determination. CCDC Deposition Numbers 2349716- 2349719 contain the supplementary crystallographic data for this paper. These data are provided free of charge by the joint Cambridge Crystallographic Data Centre and Fachinformationszentrum Karlsruhe Access Structures service www.ccdc.cam.ac.uk/structures.

A suitable single crystal of each sample was selected and mounted on a Mitegen cryoloop in a random orientation on a XtaLAB Synergy R, DW system, HyPix diffractometer. The crystals were kept around 100.00(6) K during data collection. The structures were solved with the ShelXT 2014/5[60] solution program using dual methods and Olex 2 1.3-alpha[61] as the graphical interface. The models were refined with ShelXL[62] 2018/3 using full matrix least squares minimization on F^2. All non-hydrogen atoms were refined anisotropically. Hydrogen atom positions were calculated geometrically and refined using the riding model. Data reduction, scaling and absorption corrections were performed using CrysAlisPro 1.171.40.80a.[63] Numerical absorption correction

based on gaussian integration over a multifaceted crystal model and empirical absorption correction using spherical harmonics were performed as implemented in SCALE3 ABSPACK scaling algorithm.[64]

Crystal Data of Complex 2. Single clear yellow block-shaped crystals of 2 were obtained by recrystallisation from layering hexanes on top of Et_2O. A suitable crystal 0.21 × 0.17 × 0.13 mm^3 was selected and mounted. $C_{55}H_{29}BCoF_{24}N_5O_2$, M_r = 1317.57, monoclinic, $P2_1/c$ (No. 14), a = 13.4973(10) Å, b = 19.6676(5) Å, c = 19.6806(11) Å, β = 94.942(7)°, $\alpha = \gamma = 90°$, V = 5205.0(5) $Å^3$, T = 100.00(10) K, Z = 4, Z' = 1, μ(Mo K_α) = 0.466, 82566 reflections measured, 17947 unique (R_{int} = 0.0247) which were used in all calculations. The final wR_2 was 0.1283 (all data) and R_1 was 0.0461 (I≥2 σ(I)).

Crystal Data of Complex 2_{OMe}. Single clear yellow block-shaped crystals of 2_{OMe} were obtained by recrystallisation from slow evaporation of Et_2O with a drop of MeCN. A suitable crystal 0.28 × 0.15 × 0.13 mm^3 was selected and mounted. $C_{56}H_{31}BCoF_{24.03}N_5O_3$, M_r = 1348.17, orthorhombic, $P2_12_12_1$ (No. 19), a = 16.39310(10) Å, b = 16.56500(10) Å, c = 20.4893(2) Å, $\alpha = \beta = \gamma = 90°$, V = 5563.90(7) $Å^3$, T = 100.00(11) K, Z = 4, Z' = 1, μ(Mo K_α) = 0.439, 71031 reflections measured, 18011 unique (R_{int} = 0.0218) which were used in all calculations. The final wR_2 was 0.0872 (all data) and R_1 was 0.0331 (I≥2 σ(I)).

Crystal Data of Complex ^{PPh3}2. Single clear orange block-shaped crystals of ^{PPh3}2 were obtained by recrystallisation from layering hexanes on top of Et_2O. A suitable crystal 0.19 × 0.12 × 0.08 mm^3 was selected and mounted. $C_{76.54}H_{55.08}BCoF_{24}N_5O_{1.73}P$, M_r = 1629.20, triclinic, P-1 (No. 2), a = 14.5870(2) Å, b = 16.7388(2) Å, c = 16.9022(2) Å, α = 111.0930(10)°, β = 101.0440(10)°, γ = 103.2730(10)°, V = 3572.69(8) $Å^3$, T = 100.01(10) K, Z = 2, Z' = 1, μ(Mo K_α) = 0.377, 106597 reflections measured, 24282 unique (R_{int} = 0.0278) which were used in all calculations. The final wR_2 was 0.1087 (all data) and R_1 was 0.0413 (I≥2 σ(I)).

Crystal Data of Complex ^{PMe3}2. Single clear yellow block-shaped crystals of ^{PMe3}2 were obtained by recrystallisation from layering hexanes on top of dichloromethane (DCM). A suitable crystal 0.22 × 0.13 × 0.09 mm^3 was selected and mounted. $C_{57}H_{38}BCoF_{24}N_5OP$, M_r = 1365.63, triclinic, *P*-1 (No. 2), a = 12.7418(2) Å, b = 15.2252(2) Å, c = 16.6789(2) Å, α = 92.3250(10)°, β = 107.0130(10)°, γ = 98.4410(10)°, V = 3048.58(7) Å^3, T = 100.00(10) K, Z = 2, Z' = 1, μ(Mo K$_\alpha$) = 0.425, 90080 reflections measured, 20665 unique (R_{int} = 0.0247) which were used in all calculations. The final wR_2 was 0.1241 (all data) and R_1 was 0.0449 (I≥2 σ(I)).

Conclusions

Six new Co(I) CNC pincer complexes are reported with full characterization data including single crystal X-Ray diffraction on four complexes. A change in geometry from trigonal bipyramid to square pyramid is observed upon phosphine coordination. The vibrational spectra show the electronic influence of the R group on the pincer ring with electron donor groups (OMe, Me) resulting in CO stretch that is decreased due to increasing back-bonding from an electron rich Co(I) metal center. A similar influence is observed by coordination of an electron donating phosphine ligand. Eight complexes (six new and two previously reported) have been used as catalysts for CO_2 hydrogenation with DBU as the base and LiOTf as a Lewis Acid. Herein, the three most active catalysts (all with TON >10,000) are **2**, ^{PMe3}**2**, and **1** in order of decreasing activity (Table 4). It appears that R groups on the pincer ring which are either electron donating or withdrawing tend to decrease catalytic activity which may relate to catalyst decomposition pathways. Catalyst **2** was studied further, and it appears that moderate temperature (60 °C) and pressure (20 bar of 1:1 CO_2: H_2) results in higher catalytic activity. This may relate to key steps in the catalytic cycle involving CO ligand loss and CO_2 or H_2 coordination, which are thus favored by intermediate pressures. Likewise, faster rates at intermediate temperatures may relate to having sufficient activation energy but avoiding decomposition pathways. Using these optimized conditions, nearly 40,000 TON is achieved which surpasses other studies with Co(I) catalysts.[29]

The mechanism of the reaction was computationally studied and shown to involve CO loss and H_2 coordination to generate a Co(I) dihydrogen complex. DBU then serves as a base to generate the catalytically active hydride intermediate, [(CNC)CoH(CO)], which can attack CO_2 to yield bound formate. Formate release can be promoted by assistance of either Li^+ or $[HDBU]^+$

leading to reformation of the [(CNC)CoCO] intermediate and catalyst turnover. Future studies will aim to study this mechanism further by the method of initial rates with each catalyst.

AUTHOR INFORMATION

Corresponding Authors:

*E-mail: tibor.szilvasi@ua.edu (T.S.)

*E-mail: etpapish@ua.edu (E.T.P.).

ORCID

Wenzhi Yao 0000-0002-4874-0169
Chance M. Boudreaux 0000-0003-1322-9878
Fengrui Qu 0000-0002-9975-2573
Tibor Szilvási 0000-0002-4218-1570
Elizabeth T. Papish: 0000-0002-7937-8019

ASSOCIATED CONTENT

Supporting Information

The Supporting Information is available free of charge on the ACS Publications website at DOI: xxxx.

Experimental details including spectra, single crystal X-ray diffraction figures and data tables (PDF)

Crystallographic information (CIF)

Cartesian coordinates (XYZ)

ACKNOWLEDGMENT

The authors thank the NSF (CHE-1800214 and 2102416) for funding this research. We thank NSF CHE MRI 1828078 and UA for the purchase of the SC XRD instrument. We thank NSF CHE MRI 1919906 and UA for the purchase of an NMR spectrometer. We thank Dr. Ken Belmore for assistance with the NMR

experiments. CMB thanks GAANN and AL EPSCoR for partial support. G.O. and T.S would like to acknowledge the financial support of the National Science Foundation (NSF) under grant number 2339481. G.O. would like to acknowledge the financial support of the University of Alabama Graduate School as a Graduate Council Fellow. G.O. and T.S would also like to thank the University of Alabama and the Office of Information Technology for providing high-performance computing resources.

CONFLICT OF INTEREST STATEMENT

The authors declare no conflict of interest.

References

1. Yao, W.; Boudreaux, C. M.; Wysocki, M.; Ahmed, M. K.; Qu, F.; Papish, E. T., Cobalt(I) Pincer Complexes as Catalysts for CO2 Hydrogenation to Formate. *ChemRxiv* **2024**.
2. Navarro, R. M.; Peña, M. A.; Fierro, J. L. G., Hydrogen Production Reactions from Carbon Feedstocks: Fossil Fuels and Biomass. *Chem. Rev.* **2007,** *107*, 3952-3991.
3. Eberle, U.; Felderhoff, M.; Schüth, F., Chemical and Physical Solutions for Hydrogen Storage. *Angew. Chem. Int. Ed.* **2009,** *48*, 6608-6630.
4. Filonenko, G. A.; Smykowski, D.; Szyja, B. M.; Li, G.; Szczygieł, J.; Hensen, E. J. M.; Pidko, E. A., Catalytic Hydrogenation of CO2 to Formates by a Lutidine-Derived Ru–CNC Pincer Complex: Theoretical Insight into the Unrealized Potential. *ACS Catal.* **2015,** *5*, 1145-1154.
5. Sordakis, K.; Dalebrook, A. F.; Laurenczy, G., A Viable Hydrogen Storage and Release System Based on Cesium Formate and Bicarbonate Salts: Mechanistic Insights into the Hydrogen Release Step. *ChemCatChem* **2015,** *7*, 2332-2339.
6. Wang, W.-H.; Himeda, Y.; Muckerman, J. T.; Manbeck, G. F.; Fujita, E., CO2 Hydrogenation to Formate and Methanol as an Alternative to Photo- and Electrochemical CO2 Reduction. *Chem. Rev.* **2015,** *115*, 12936-12973.
7. Liu, Q.; Wu, L.; Gülak, S.; Rockstroh, N.; Jackstell, R.; Beller, M., Towards a Sustainable Synthesis of Formate Salts: Combined Catalytic Methanol Dehydrogenation and Bicarbonate Hydrogenation. *Angew. Chem. Int. Ed.* **2014,** *53*, 7085-7088.
8. Siek, S.; Burks, D. B.; Gerlach, D. L.; Liang, G.; Tesh, J. M.; Thompson, C. R.; Qu, F.; Shankwitz, J. E.; Vasquez, R. M.; Chambers, N. S.; Szulczewski, G. J.; Grotjahn, D. B.; Webster, C. E.; Papish, E. T., Iridium and Ruthenium Complexes of NHC and Pyridinol Derived Chelates as Catalysts for Aqueous Carbon Dioxide Hydrogenation and Formic Acid Dehydrogenation: The Role of the Alkali Metal. *Organometallics* **2017,** *36*, 1091-1106.
9. Jessop, P. G.; Ikariya, T.; Noyori, R., Homogeneous Hydrogenation of Carbon Dioxide. *Chem. Rev.* **1995,** *95*, 259-272.
10. Jessop, P. G.; Joó, F.; Tai, C.-C., Recent advances in the homogeneous hydrogenation of carbon dioxide. *Coord. Chem. Rev.* **2004,** *248*, 2425-2442.
11. Leitner, W., Carbon Dioxide as a Raw Material: The Synthesis of Formic Acid and Its Derivatives from CO2. *Angew. Chem., Int. Ed.* **1995,** *34*, 2207-2221.

12. Wang, W.; Wang, S.; Ma, X.; Gong, J., Recent advances in catalytic hydrogenation of carbon dioxide. *Chem. Soc. Rev.* **2011,** *40*, 3703-3727.
13. Siegel, R. E.; Pattanayak, S.; Berben, L. A., Reactive Capture of CO2: Opportunities and Challenges. *ACS Catal.* **2023,** *13*, 766-784.
14. Tanaka, R.; Yamashita, M.; Nozaki, K., Catalytic Hydrogenation of Carbon Dioxide Using Ir(III)−Pincer Complexes. *J. Am. Chem. Soc.* **2009,** *131*, 14168-14169.
15. Schmeier, T. J.; Dobereiner, G. E.; Crabtree, R. H.; Hazari, N., Secondary Coordination Sphere Interactions Facilitate the Insertion Step in an Iridium(III) CO2 Reduction Catalyst. *J. Am. Chem. Soc.* **2011,** *133*, 9274-9277.
16. Munshi, P.; Main, A. D.; Linehan, J. C.; Tai, C.-C.; Jessop, P. G., Hydrogenation of Carbon Dioxide Catalyzed by Ruthenium Trimethylphosphine Complexes: The Accelerating Effect of Certain Alcohols and Amines. *J. Am. Chem. Soc.* **2002,** *124*, 7963-7971.
17. Tanaka, R.; Yamashita, M.; Chung, L. W.; Morokuma, K.; Nozaki, K., Mechanistic Studies on the Reversible Hydrogenation of Carbon Dioxide Catalyzed by an Ir-PNP Complex. *Organometallics* **2011,** *30*, 6742-6750.
18. Hutschka, F.; Dedieu, A.; Eichberger, M.; Fornika, R.; Leitner, W., Mechanistic Aspects of the Rhodium-Catalyzed Hydrogenation of CO2 to Formic AcidA Theoretical and Kinetic Study†,‖. *J. Am. Chem. Soc.* **1997,** *119*, 4432-4443.
19. Ocansey, E.; Darkwa, J.; Makhubela, B. C. E., Iridium and Palladium CO2 Hydrogenation in Water by Catalyst Precursors with Electron-Rich Tetrazole Ligands. *Organometallics* **2020,** *39*, 3088-3098.
20. Inoue, Y.; Izumida, H.; Sasaki, Y.; Hashimoto, H., Catalytic fixation of carbon dioxide to formic acid by transition-metal complexes under mild conditions. *Chem. Lett.* **1976,** *5*, 863-864.
21. Jessop, P. G.; Ikariya, T.; Noyori, R., Homogeneous catalytic hydrogenation of supercritical carbon dioxide. *Nature* **1994,** *368*, 231-233.
22. Huff, C. A.; Kampf, J. W.; Sanford, M. S., Role of a Noninnocent Pincer Ligand in the Activation of CO2 at (PNN)Ru(H)(CO). *Organometallics* **2012,** *31*, 4643-4645.
23. Vogt, M.; Gargir, M.; Iron, M. A.; Diskin-Posner, Y.; Ben-David, Y.; Milstein, D., A New Mode of Activation of CO2 by Metal-Ligand Cooperation with Reversible C-C and M-O Bond Formation at Ambient Temperature. *Chem. - Eur. J.* **2012,** *18*, 9194-9197, S9194/1-S9194/37.
24. Sanz, S.; Benítez, M.; Peris, E., A New Approach to the Reduction of Carbon Dioxide: CO 2Reduction to Formate by Transfer Hydrogenation in iPrOH. *Organometallics* **2010,** *29*, 275-277.
25. Himeda, Y.; Onozawa-Komatsuzaki, N.; Sugihara, H.; Kasuga, K., Simultaneous Tuning of Activity and Water Solubility of Complex Catalysts by Acid−Base Equilibrium of Ligands for Conversion of Carbon Dioxide. *Organometallics* **2007,** *26*, 702-712.
26. Himeda, Y.; Miyazawa, S.; Hirose, T., Interconversion between Formic Acid and H2/CO2 using Rhodium and Ruthenium Catalysts for CO2 Fixation and H2 Storage. *ChemSusChem* **2011,** *4*, 487-493.
27. Bertini, F.; Glatz, M.; Gorgas, N.; Stöger, B.; Peruzzini, M.; Veiros, L. F.; Kirchner, K.; Gonsalvi, L., Carbon dioxide hydrogenation catalysed by well-defined Mn(i) PNP pincer hydride complexes. *Chem. Sci.* **2017,** *8*, 5024-5029.
28. Zhang, Y.; MacIntosh, A. D.; Wong, J. L.; Bielinski, E. A.; Williard, P. G.; Mercado, B. Q.; Hazari, N.; Bernskoetter, W. H., Iron catalyzed CO2 hydrogenation to formate enhanced by Lewis acid co-catalysts. *Chem. Sci.* **2015,** *6*, 4291-4299.
29. Spentzos, A. Z.; Barnes, C. L.; Bernskoetter, W. H., Effective Pincer Cobalt Precatalysts for Lewis Acid Assisted CO 2Hydrogenation. *Inorg. Chem.* **2016,** *55*, 8225–8233.
30. Burgess, S. A.; Grubel, K.; Appel, A. M.; Wiedner, E. S.; Linehan, J. C., Hydrogenation of CO2 at Room Temperature and Low Pressure with a Cobalt Tetraphosphine Catalyst. *Inorg. Chem.* **2017,** *56*, 8580-8589.
31. Federsel, C.; Ziebart, C.; Jackstell, R.; Baumann, W.; Beller, M., Catalytic Hydrogenation of Carbon Dioxide and Bicarbonates with a Well-Defined Cobalt Dihydrogen Complex. *Chem. Eur. J.* **2012,** *18*, 72-75.

32. Burgess, S. A.; Kendall, A. J.; Tyler, D. R.; Linehan, J. C.; Appel, A. M., Hydrogenation of CO2 in Water Using a Bis(diphosphine) Ni–H Complex. *ACS Catal.* **2017,** *7*, 3089-3096.
33. Zall, C.; Linehan, J.; Appel, A., A Molecular Copper Catalyst for Hydrogenation of CO2 to Formate. *ACS Catal.* **2015,** *5*, 150805132443001.
34. Trivedi, M.; Kumar, A.; Husain, A.; Rath, N. P., Copper(I) Complexes Containing PCP Ligand Catalyzed Hydrogenation of Carbon Dioxide to Formate under Ambient Conditions. *Inorg. Chem.* **2021,** *60*, 4385-4396.
35. Boudreaux, C. M.; Nugegoda, D.; Yao, W.; N., L.; Frey, N. C.; Li, Q.; Qu, F.; Zeller, M.; Webster, E.; Delcamp, J. H.; Papish, E. T., Low Valent Cobalt(I) CNC Pincer Complexes as Catalysts for Light Driven Carbon Dioxide Reduction. *ACS Catal.* **2022,** *12*, 8718-8728.
36. Burks, D. B.; Davis, S.; Lamb, R. W.; Liu, X.; Rodrigues, R. R.; Liyanage, N. P.; Sun, Y.; Webster, C. E.; Delcamp, J. H.; Papish, E. T., Nickel(II) pincer complexes demonstrate that the remote substituent controls catalytic carbon dioxide reduction. *Chem. Commun.* **2018,** *54*, 3819-3822.
37. Manafe, S. Y.; Le, N.; Lambert, E. C.; Curiac, C.; Nugegoda, D.; Das, S.; Hunt, L. A.; Qu, F.; Whitt, L. M.; Fedin, I.; Hammer, N. I.; Webster, C. E.; Delcamp, J. H.; Papish, E. T., Sensitized and Self-Sensitized Photocatalytic CO2 Reduction to HCO2– and CO under Visible Light with Ni(II) CNC-Pincer Catalysts. *ACS Catal.* **2024**, 6589-6602.
38. Yao, W.; Das, S.; DeLucia, N. A.; Qu, F.; Boudreaux, C. M.; Vannucci, A. K.; Papish, E. T., Determining the Catalyst Properties That Lead to High Activity and Selectivity for Catalytic Hydrodeoxygenation with Ruthenium Pincer Complexes. *Organometallics* **2020,** *39*, 662-669.
39. Das, S.; Nugegoda, D.; Qu, F.; Boudreaux, C. M.; Burrow, P. E.; Figgins, M. T.; Lamb, R. W.; Webster, C. E.; Delcamp, J. H.; Papish, E. T., Structure Function Relationships in Ruthenium Carbon Dioxide Reduction Catalysts with CNC Pincers Containing Donor Groups. *Eur. J. Inorg. Chem.* **2020,** *2020*, 2709-2717.
40. Mika, L. T.; Tuba, R.; Tóth, I.; Pitter, S.; Horváth, I. T., Molecular Mapping of the Catalytic Cycle of the Cobalt-Catalyzed Hydromethoxycarbonylation of 1,3-Butadiene in the Presence of Pyridine in Methanol. *Organometallics* **2011,** *30*, 4751-4764.
41. Hollingsworth, R. L.; Beattie, J. W.; Grass, A.; Martin, P. D.; Groysman, S.; Lord, R. L., Reactions of dicobalt octacarbonyl with dinucleating and mononucleating bis(imino)pyridine ligands. *Dalton Trans.* **2018,** *47*, 15353-15363.
42. Addison, A. W.; Rao, T. N.; Reedijk, J.; Rijn, J. v.; Verschoor, G. C., Synthesis, structure, and spectroscopic properties of copper(II) compounds containing nitrogen–sulphur donor ligands; the crystal and molecular structure of aqua[1,7-bis(N-methylbenzimidazol-2-yl)-2,6-dithiaheptane]copper(II) perchlorate. *J. Chem. Soc., Dalton Trans.* **1984**, 1349 - 1356.
43. Das, S.; Rodrigues, R. R.; Lamb, R. W.; Qu, F.; Reinheimer, E.; Boudreaux, C. M.; Webster, C. E.; Delcamp, J. H.; Papish, E. T., Highly Active Ruthenium CNC Pincer Photocatalysts for Visible-Light-Driven Carbon Dioxide Reduction. *Inorg. Chem.* **2019,** *58*, 8012-8020.
44. Boudreaux, C. M.; Liyanage, N. P.; Shirley, H.; Siek, S.; Gerlach, D. L.; Qu, F.; Delcamp, J. H.; Papish, E. T., Ruthenium(II) complexes of pyridinol and N-heterocyclic carbene derived pincers as robust catalysts for selective carbon dioxide reduction. *Chem. Commun.* **2017,** *53*, 11217-11220.
45. Pérez, E. R.; da Silva, M. O.; Costa, V. C.; Rodrigues-Filho, U. P.; Franco, D. W., Efficient and clean synthesis of N-alkyl carbamates by transcarboxylation and O-alkylation coupled reactions using a DBU–CO2 zwitterionic carbamic complex in aprotic polar media. *Tetrahedron Letters* **2002,** *43*, 4091-4093.
46. Heldebrant, D. J.; Jessop, P. G.; Thomas, C. A.; Eckert, C. A.; Liotta, C. L., The Reaction of 1,8-Diazabicyclo[5.4.0]undec-7-ene (DBU) with Carbon Dioxide. *The Journal of Organic Chemistry* **2005,** *70*, 5335-5338.
47. Dawe, L. N.; Karimzadeh-Younjali, M.; Dai, Z.; Khaskin, E.; Gusev, D. G., The Milstein Bipyridyl PNN Pincer Complex of Ruthenium Becomes a Noyori-Type Catalyst under Reducing Conditions. *J. Am. Chem. Soc.* **2020,** *142*, 19510-19522.

48. Bielinski, E. A.; Förster, M.; Zhang, Y.; Bernskoetter, W. H.; Hazari, N.; Holthausen, M. C., Base-Free Methanol Dehydrogenation Using a Pincer-Supported Iron Compound and Lewis Acid Co-catalyst. *ACS Catal.* **2015,** *5*, 2404-2415.
49. Fulmer, G. R.; Miller, A. J. M.; Sherden, N. H.; Gottlieb, H. E.; Nudelman, A.; Stoltz, B. M.; Bercaw, J. E.; Goldberg, K. I., NMR Chemical Shifts of Trace Impurities: Common Laboratory Solvents, Organics, and Gases in Deuterated Solvents Relevant to the Organometallic Chemist. *Organometallics* **2010,** *29*, 2176-2179.
50. Frisch, M. J. T., G. W.; Schlegel, H. B.; Scuseria, G. E.; Robb, M. A.; Cheeseman, J. R.; Scalmani, G.; Barone, V.; Petersson, G. A.; Nakatsuji, H.; Li, X.; Caricato, M.; Marenich, A. V.; Bloino, J.; Janesko, B. G.; Gomperts, R.; Mennucci, B.; Hratchian, H. P.; Ortiz, J. V.; Izmaylov, A. F.; Sonnenberg, J. L.; Williams; Ding, F.; Lipparini, F.; Egidi, F.; Goings, J.; Peng, B.; Petrone, A.; Henderson, T.; Ranasinghe, D.; Zakrzewski, V. G.; Gao, J.; Rega, N.; Zheng, G.; Liang, W.; Hada, M.; Ehara, M.; Toyota, K.; Fukuda, R.; Hasegawa, J.; Ishida, M.; Nakajima, T.; Honda, Y.; Kitao, O.; Nakai, H.; Vreven, T.; Throssell, K.; Montgomery Jr., J. A.; Peralta, J. E.; Ogliaro, F.; Bearpark, M. J.; Heyd, J. J.; Brothers, E. N.; Kudin, K. N.; Staroverov, V. N.; Keith, T. A.; Kobayashi, R.; Normand, J.; Raghavachari, K.; Rendell, A. P.; Burant, J. C.; Iyengar, S. S.; Tomasi, J.; Cossi, M.; Millam, J. M.; Klene, M.; Adamo, C.; Cammi, R.; Ochterski, J. W.; Martin, R. L.; Morokuma, K.; Farkas, O.; Foresman, J. B.; Fox, D. J., Gaussian 16 Rev. C.01. *Wallingford, CT,* **2016**.
51. Neese, F., Software update: The ORCA program system—Version 5.0. *Wiley Interdisciplinary Reviews: Computational Molecular Science* **2022,** *12*, e1606.
52. Riplinger, C.; Sandhoefer, B.; Hansen, A.; Neese, F., Natural triple excitations in local coupled cluster calculations with pair natural orbitals. *The Journal of chemical physics* **2013,** *139*.
53. Bannwarth, C.; Ehlert, S.; Grimme, S., GFN2-xTB—An Accurate and Broadly Parametrized Self-Consistent Tight-Binding Quantum Chemical Method with Multipole Electrostatics and Density-Dependent Dispersion Contributions. *J. Chem. Theory Comput.* **2019,** *15*, 1652-1671.
54. Grimme, S., Exploration of Chemical Compound, Conformer, and Reaction Space with Meta-Dynamics Simulations Based on Tight-Binding Quantum Chemical Calculations. *J. Chem. Theory Comput.* **2019,** *15*, 2847-2862.
55. Bannwarth, C.; Caldeweyher, E.; Ehlert, S.; Hansen, A.; Pracht, P.; Seibert, J.; Spicher, S.; Grimme, S., Extended tight-binding quantum chemistry methods. *WIREs Computational Molecular Science* **2021,** *11*, e1493.
56. Marenich, A. V.; Cramer, C. J.; Truhlar, D. G., Universal solvation model based on solute electron density and on a continuum model of the solvent defined by the bulk dielectric constant and atomic surface tensions. *The Journal of Physical Chemistry B* **2009,** *113*, 6378-6396.
57. Chai, J.-D.; Head-Gordon, M., Long-range corrected hybrid density functionals with damped atom–atom dispersion corrections. *Physical Chemistry Chemical Physics* **2008,** *10*, 6615-6620.
58. Weigend, F.; Ahlrichs, R., Balanced basis sets of split valence, triple zeta valence and quadruple zeta valence quality for H to Rn: Design and assessment of accuracy. *Physical Chemistry Chemical Physics* **2005,** *7*, 3297-3305.
59. Luchini, G.; Alegre-Requena, J. V.; Funes-Ardoiz, I.; Paton, R. S., GoodVibes: automated thermochemistry for heterogeneous computational chemistry data. *F1000Research* **2020,** *9*, 291.
60. Sheldrick, G. M., SHELXT-Integrated Space-Group and Crystal-Structure Determination. *Acta Crystallographica Section A* **2015,** *71*, 3-8.
61. Dolomanov, O. V.; Bourhis, L. J.; Gildea, R. J.; Howard, J. A. K.; Puschmann, H., OLEX2: A Complete Structure Solution, Refinement and Analysis Program. *Journal of Applied Crystallography* **2009,** *42*, 339-341.
62. Sheldrick, G. M., Crystal structure refinement with SHELXL. *Structural Chemistry* **2014,** *71*, 3-8.
63. CrysAlisPro *Rigaku Oxford Diffraction*, V1.171.40.80a; 2020.
64. ABSPACK, S. *A Rigaku Oxford Diffraction program for Absorption Corrections, Rigaku Oxford Diffraction*, 2017.